Crafting the strain state in epitaxial thin films: A case study of $CoFe_2O_4$ films on $Pb(Mg,Nb)O_3$-$PbTiO_3$

Zhiguang Wang,[1,*] Yaojin Wang,[1] Haosu Luo,[2] Jiefang Li,[1] and D. Viehland[1]

[1]*Department of Materials Science and Engineering, Virginia Tech, Blacksburg, Virginia 24061, USA*

[2]*State Key Laboratory of High Performance Ceramics and Superfine Microstructure, Shanghai Institute of Ceramics, Chinese Academy of Sciences, Shanghai 201800, China*

(Received 1 June 2014; revised manuscript received 25 September 2014; published 9 October 2014)

The strain dependence of electric and magnetic properties has been widely investigated, both from a fundamental science perspective and an applications point of view. Electromechanical coupling through field-induced polarization rotation (PRO) and polarization reorientation (PRE) in piezoelectric single crystals can provide an effective strain in film/substrate epitaxial heterostructures. However, the specific pathway of PRO and PRE is a complex thermodynamic process, depending on chemical composition, temperature, electric field, and mechanical load. Here, systematic studies of the temperature-dependent field-induced phase transitions in $Pb(Mg,Nb)O_3$-$PbTiO_3$ single crystals with different initial phase and orientation configurations have been performed. Different types of strains, volatile/nonvolatile and biaxial/uniaxial, have been measured by both macroscopic and *in situ* x-ray diffraction techniques. In addition, the strain state of epitaxial Mn-doped $CoFe_2O_4$ thin films was examined by magnetic anisotropy measurements, where a giant magnetoelectric coupling has been demonstrated.

DOI: 10.1103/PhysRevB.90.134103 PACS number(s): 81.15.Fg, 77.84.Lf, 77.80.bg, 77.55.Nv

I. INTRODUCTION

It is well known that both electric and magnetic properties of crystalline materials depend on their lattice parameters and the symmetry of their unit cell [1–3]. Strain engineering has been adopted to modulate the properties of a vast number of functional materials, including strained oxides, strained atomic sheets, strained catalysts, and strained silicon technologies [4].

Recent advances in the growth of epitaxial thin films on single-crystal substrates provide additional freedom in controlling the strain condition in thin films [5–7]. A layer-on-layer growth-induced strong chemical bonding guarantees a near-perfect strain transfer from substrate to film, whether an intrinsic lattice mismatch or an electrically controlled lattice deformation. With regards to strain engineering of ferroelectric thin films, the Curie temperature can be shifted hundreds of degrees and the saturation polarization can be increased by more than a factor of 2 [2,8,9]. In ferromagnetic films grown on piezoelectric substrates, the magnetic easy axis can be rotated and the ferromagnetic resonance frequency can be shifted by the electrically induced strain of the substrate [6,10,11]. In superconductor films, the superconducting transition temperature can be shifted by strain [12,13]. In strongly correlated materials, the electrical conductivity can be changed by several orders due to strain from the substrate [1].

Piezoelectric single crystals have been widely used as substrates due to a good crystal lattice parameter matching with most functional oxides and due to their large electromechanical coupling coefficients [5,14,15]. Significant effort has been placed on the study of electric-field-induced strains in Pb-based piezoelectric crystals due to their applications in sensors and transducers. Most of these investigations have focused on strain evolution along the direction of the electric field, whereas the strain along the in-plane directions is the key factor for strain modulation of epitaxial films. One might anticipate that the in-plane strain can be estimated from the out-of-plane one based on Poisson's ratio. However, detailed studies of the orientation-dependent mechanical properties of perovskites have shown an abnormal Poisson's ratio and compressibility that depend on both orientation and unit cell shape [6,16]. Moreover, previous studies treated the piezoelectric substrate as a linear strain source under application of external electric field, which is only true within a small range of electric fields over which phase transformations do not occur.

Here, $Pb(Mg,Nb)O_3$-$PbTiO_3$ (PMN-PT) substrates were selected with different initial phases (rhombohedral or tetragonal: *R* or *T* for short) and different out-of-plane orientations ($\langle 001\rangle_c$ or $\langle 011\rangle_c$, where "c" indicates pseudocubic notation). The temperature and electric-field dependences of the phase transformations were thoroughly investigated by both macroscopic strain and microscopic *in situ* x-ray diffraction (XRD) techniques. The strain effect was examined by measurement of the magnetic anisotropy of the Mn-doped $CoFe_2O_4$ (MCFO) thin films epitaxially grown on the substrates [17].

II. EXPERIMENT

Three different single crystals were used in this study: $\langle 001\rangle_c$-oriented PMN-30PT, $\langle 001\rangle_c$-oriented PMN-40PT, and $\langle 011\rangle_c$-oriented PMN-29.5PT. To examine the strain effect on epitaxial films, MCFO thin films with thickness ~400 nm were deposited on PMN-PT substrates by pulsed laser deposition. Detailed growth process can be found in a previous report [6]. The crystal structure of the single-crystal substrates and films was determined using a Philips X'pert high-resolution x-ray diffractometer. The macroscopic strain curves were measured with capacitive displacement sensor under different electric fields. Magnetic hysteresis (*M*-*H*) loops were measured with a Lakeshore 7300 series vibrating sample magnetometer (VSM)

*Author to whom correspondence should be addressed: zgwang@vt.edu

system at room temperature, where the samples were connected to a Bertan high-voltage power supply (210–20R) in order to apply electric fields. The field-induced strain from the piezoelectric PMN-PT substrate is transferred to the epitaxial MCFO thin film, thus changing the magnetic anisotropy distribution in the MCFO layer due to the well-known magnetoelectric (ME) effect of the heterostructure [14,15,17–23].

III. RESULTS AND DISCUSSION

Figure 1 shows the three factors that determine the type of strain that can be obtained from PMN-PT substrates. First, the initial phase configuration of the PMN-PT substrate at room temperature is defined by the composition of (1–x)PMN-xPT. PMN-PT with low-PT contents ($x < 0.3$) has a rhombohedral (R) structure with P_s oriented along ⟨111⟩ directions. A mixture of R, orthorhombic (O), monoclinic (M), and tetragonal (T) phases is found for $0.3 < x < 0.38$ [24]. For $x > 0.38$, the stable phase is tetragonal. Application of electric field can change the polarization direction, distorting the unit cell to a different symmetry. This in turn results in a strain in the epitaxial film. Field-induced polarization rotation depends on both the direction along which the electric field is applied and the ambient temperature conditions [25].

Figure 2 shows the electric-field-dependent polarization rotation pathways and resultant strain conditions for PMN-PT of several different orientations and different initial phases. The R phase has eight equivalent polarization directions [Fig. 2(a)]. For $E//\langle 001\rangle_c$, the polarization will rotate away from $\langle 111\rangle_c$ towards E within monoclinic A (M_C) and then C (M_C) phases. At sufficiently high E, an induced $R \rightarrow T$ transition occurs [26], resulting in a pseudouniform strain in the heteroepitaxial film. The polarization as well as the long axis direction of the field-induced T phase is along the out-of-plane direction, therefore, the field-induced in-plane strain is compressive. In the T phase, there are six equivalent polarization directions [Fig. 2(b)]. The ferroelectric domains can be divided into two types: c domains whose polarization lies along the out-of-plane direction and a domains whose polarization is in plane. By application of $E//\langle 001\rangle_c$, a domains will transform to c domains, inducing a large strain in the film on the crystal substrate [27]. This type of strain is strongly related to the original local domain state: for a-domain

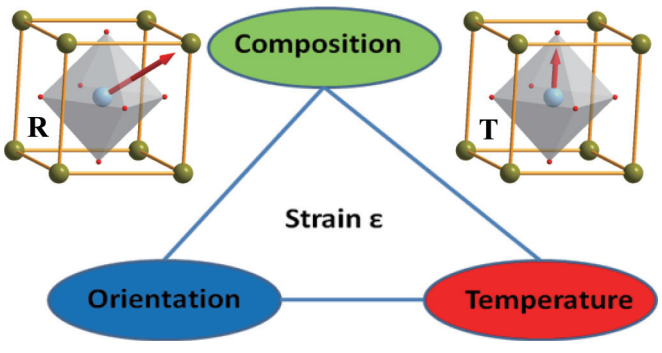

FIG. 1. (Color online) Schematic of the three factors that determine the field-induced strain amplitude and stability.

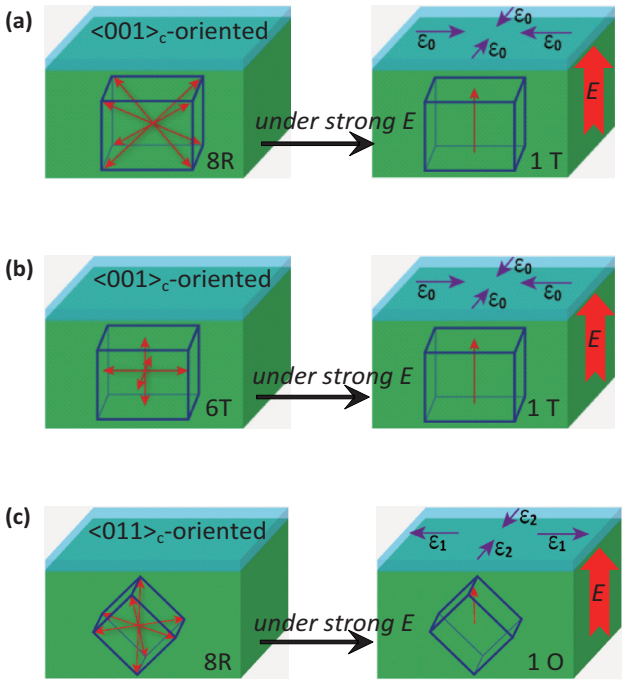

FIG. 2. (Color online) Schematic of the electric-field-induced polarization rotation and reorientation in PMN-PT single crystals and the resultant strains with different directivity: (a) $\langle 001\rangle_c$-oriented PMN-30PT; (b) $\langle 001\rangle_c$-oriented PMN-40PT; (c) $\langle 011\rangle_c$-oriented PMN-29.5PT.

regions, the a- to c-domain transition results in a large strain, whereas the original c-domain regions exhibit much smaller strain. For $\langle 011\rangle_c$-oriented R-phase crystals, there are eight equivalent polarization directions [Fig. 2(c)]. Under $E//\langle 011\rangle_c$, the polarization will rotate away from the $\langle 111\rangle_c$ in a M_B phase towards $\langle 011\rangle_c$. Under a sufficiently high E, a monodomain O phase will be induced [6]. During this $R \rightarrow M_B \rightarrow O$ phase transition, a uniaxial strain is generated in the heteroepitaxial film, which is compressive along in-plane (IP) $\langle 100\rangle_c$ and tensile along IP $\langle 0{-}11\rangle_c$ [Fig. 2(c)].

Figure 3 shows macroscopic unipolar strain curves for $\langle 001\rangle_c$ PMN-30PT crystals at different temperatures. A phase transformation sequence of $R \rightarrow M_A \rightarrow M_C \rightarrow T$ has been widely reported in PMN-PT for $E//\langle 001\rangle_c$ [28,29]. During P rotation in the monoclinic phases, the out-of-plane (OP) component of P continuously increases whereas the IP one decreases. Thus, a uniform compressive strain is induced in a heteroepitaxial thin film deposited on such a PMN-PT substrate. Three different stages of the strain process can be identified, indicating different phase transformation steps [Fig. 3(a)]. The shape changes of the $R \rightarrow M_A \rightarrow M_C$ phase transformation sequence are tempered due to the relatively flat free energy profile across these phases [28]; however, the $M_C \rightarrow T$ phase transformation induces a significant distortion of the unit cell and consequently a sharp increase of ε. We denote the field at which the $M_C \rightarrow T$ transformation occurs with a large change in ε as E_{M-T}. Figure 3(b) summarizes the relationship between E_{M-T} and temperature. Since the T phase is the higher-temperature phase, the $M_C \rightarrow T$ transformation becomes easier with increasing temperature, and thus E_{M-T} is decreased. When used as a substrate,

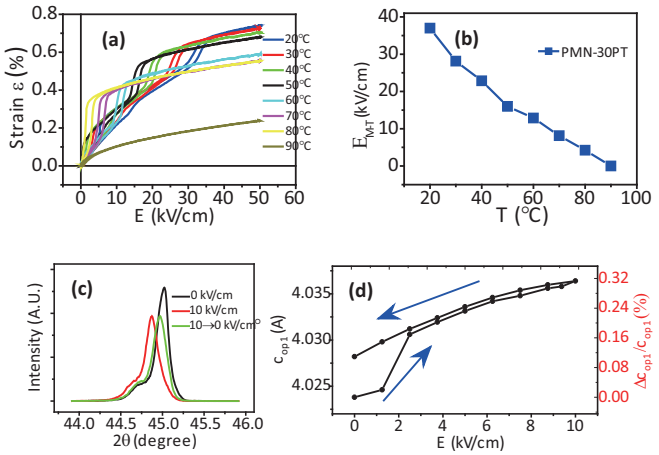

FIG. 3. (Color online) (a) Field-induced OP strain at different temperatures in the $\langle 001\rangle_c$-oriented PMN-30PT. (b) Temperature-dependent threshold electric field for $M_C \rightarrow T$ phase transformation. (c) XRD characterization of the $\langle 002\rangle_c$ peaks shifted by external electric fields. (d) Electric-field-dependent OP crystal lattice parameters.

this shows that a much larger strain can be transferred to a heteroepitaxial layer by relatively smaller fields by proper selection of temperature. Figure 3(c) shows XRD line scans under different E where a left shift can clearly be identified due to the elongation of the crystal lattice parameter with increasing E. The *in situ* equivalent out-of-plane crystal lattice parameter (c_{op1}) as a function of E is shown in Fig. 3(d). The value of c_{op1} was calculated by the formula

$$c_{\mathrm{op1}} = 2d = \frac{\lambda}{2\sin(\theta)}, \tag{1}$$

where λ is the wavelength of the x-ray source with value $\lambda = 1.5406$ Å. For as-grown PMN-30PT, $c_{\mathrm{op1}} = 1.5604/\sin(45.02°/2) = 4.024$ Å, which subsequently increased in value with increasing E. The first jump near $E = 2$ kV/cm represents the $R \rightarrow M_A$ transformation. After entering the monoclinic phase region, the ε-E response was a near-linear curve as long as E was not sufficient to induce a $M_C \rightarrow T$ transition near $E \approx 30$ kV/cm. After removal of E, the M_A phase configuration is maintained, resulting in an irreversible increase of c_{op1}. The strain can be calculated by the equation

$$\varepsilon = \frac{\Delta c_{\mathrm{op1}}}{c_{\mathrm{op1}}} = \frac{c_{\mathrm{op1}}@10\ \mathrm{kV/cm} - c_{\mathrm{op1}}@0\ \mathrm{kV/cm}}{c_{\mathrm{op1}}@0\ \mathrm{kV/cm}}. \tag{2}$$

Accordingly, on the first cycle of the unipolar ε-E curve, the field-induced strain reached a value of $\varepsilon = 0.32\%$ whereas on the second cycle, it reached only $\varepsilon = 0.2\%$. This difference is due to the irreversible $R \rightarrow M_A$ transformation. The first time field-dependent in-plane strain is complex due to the complex $R \rightarrow M_A \rightarrow M_C$ phase transition sequence. A reversible in-plane strain $\varepsilon_{\mathrm{ip}} = 0.028\%$ @10 kV/cm can be obtained from the microscopic XRD measurements, which can then subsequently be transferred to a heteroepitaxial magnetic layer for the modulation of the magnetic anisotropy. The ME effect has been measured for MCFO thin film on $\langle 001\rangle_c$-oriented PMN-30PT, where a change in the remanent magnetization has been well recognized as a function of the field-induced in-plane strain (see Supplemental Material [30]).

Figure 4 shows the details of E-dependent P reorientation in $\langle 001\rangle_c$-oriented PMN-40PT which has a stable T phase ($a = b < c$ and $\alpha = \beta = \gamma = 90°$). As-grown PMN-40PT has six possible equivalent polarization directions, as shown in Fig. 4(a). We denote the domains with P along IP as a domains, and these along OP as c domains. For the a domains, the two in-plane crystal lattice parameters are a and c, whereas the out-of-plane one is a. For the c domains, both in-plane lattice parameters are a, whereas the out-of-plane one is c. After

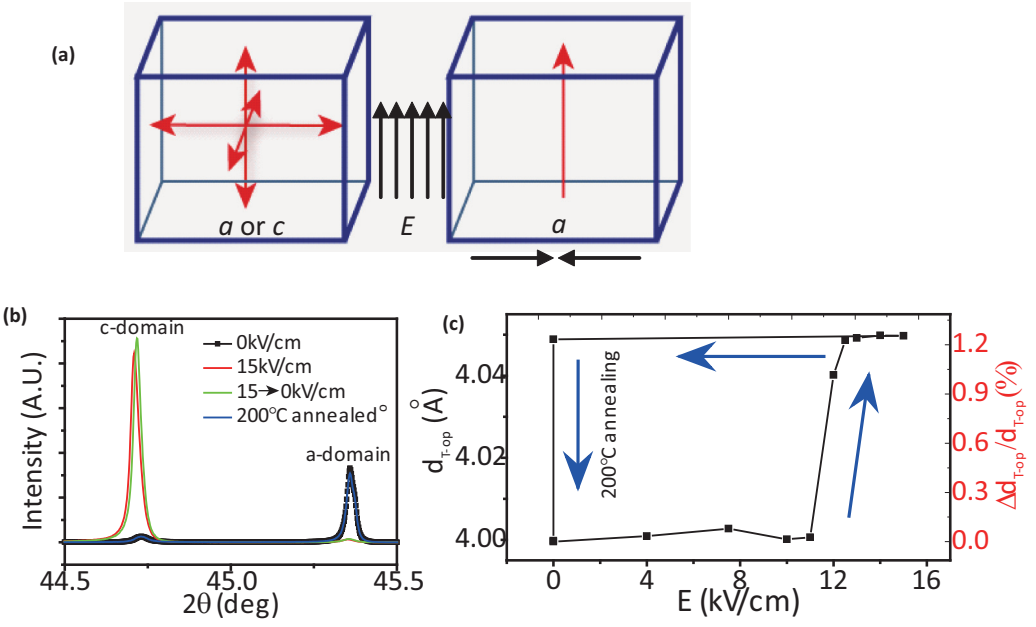

FIG. 4. (Color online) (a) Field-induced polarization reorientation in $\langle 001\rangle_c$-oriented PMN-40PT. (b) XRD results of PMN-40PT under different electric fields. (c) Electric-field-dependent OP d-spacing parameter.

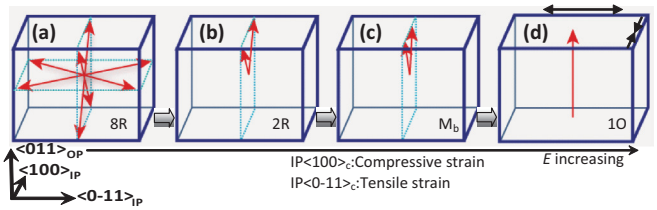

FIG. 5. (Color online) Field-induced polarization rotation in $\langle 011\rangle_c$-oriented PMN-29.5PT.

$a \rightarrow c$ domain reorientation, a large in-plane compressive strain was induced. Figure 4(b) shows XRD measurements of the E-dependent domain configuration (ratio of a and c domains) in PMN-40PT. The measurement was performed along the OP direction; thus the (002)c peak with a larger d-spacing parameter comes from c domains, whereas (200)c comes from a domains. The tetragonal crystal lattice parameters were calculated to be (a, c) = (3.996, 4.051 Å). Thus, for the completed $a \rightarrow c$ domain rotation, a compressive strain of $\varepsilon = (a-c)/c \approx -1.36\%$ is obtained along IP. The total IP compressive strain value is the statistical average value over all the domains. The OP tensile strain can then be estimated by the a-domain/c-domain ratio before and after application of E based on the intensity of the diffraction peaks from each domain component, as shown in Fig. 4(c). A tensile OP strain of $\varepsilon = 1.2\%$ and a compressive IP strain of $\varepsilon = -0.6\%$ can thus be obtained.

Again, the ME effect has been studied after depositing epitaxial MCFO thin film on $\langle 001\rangle_c$-oriented PMN-40PT, where a much larger change in the remanent magnetization has been observed. However, the field-induced in-plane strain could not relax after removal of the external field, meaning that the magnetization tuning is a one-time effect (see Supplemental Material [31]).

Figure 5 shows the E dependence of the P rotation in $\langle 011\rangle_c$-oriented PMN-29.5PT. Initially the crystal had a stable R-phase with eight possible equivalent polarization directions, as shown in Fig. 5(a). Under an out-of-plane E, a transformation sequence of $R \rightarrow M_B \rightarrow O$ has been widely reported [32–36]. The application of E degenerates the eight domain states into the two acclivous ones, as shown in Fig. 5(b). With further increase of E, the two M_B domain states transform to a single domain state that has a stable monodomain O phase, as shown in Fig. 5(d). Upon removal of E, the stable phase relaxes back to M_B with two domain states. Please note that this relaxation back to a polydomain M phase is strongly composition dependent [6]; with slight increase of PT content, the O phase can be retained upon removal of E.

Figure 6(a) shows XRD line scans for the E-dependent domain configuration of PMN-29.5PT. Measurements were performed along OP, and the R-phase (022) peak indicates an interplanar spacing of $d_1 = 2.845$ Å. Under $E = 10$ kV/cm, a monodomain O-phase condition was induced with an interplanar spacing of $d_2 = 2.851$ Å. The out-of-plane strain was determined to be $\varepsilon_{op} = \Delta d/d = (2.851–2.845)/2.845 = 0.21\%$ based on the changes in the (022) interplanar spacing, which was further confirmed to be $\varepsilon_{op} = 0.26\%$ based upon

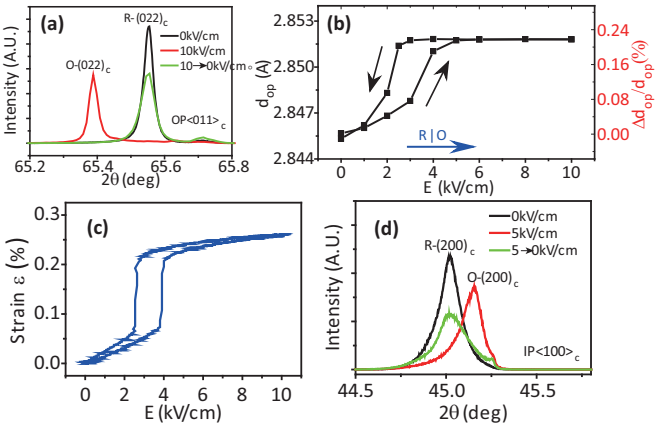

FIG. 6. (Color online) (a) XRD results of $\langle 011\rangle_c$ PMN-29.5PT under different electric fields. (b) Electric-field-dependent OP d-spacing parameter. (c) Field-dependent macroscopic strain curve. (d) XRD results along IP$\langle 100\rangle_c$ under different electric fields.

the macroscopic strain measurement, as shown in Figs. 6(b) and 6(c). Figure 6(d) shows XRD line scans under different E. For $E = 0$ kV/cm, a diffraction peak of R-(200)c ($2\theta = 42.02°$) was observed, which then shifted with increasing E ($0 \rightarrow 5$ kV/cm) to O-(200)c ($2\theta = 42.156°$). Upon removal of E, the diffraction peak shifted back to the original position due to the relaxation of the field-induced O phase. Therefore, a reversible IP strain of $\varepsilon_{ip} = \Delta d/d = 0.56\%$, which is two times that of ε_{op}, can be obtained with $E = 5$ kV/cm. More importantly, this is a transverse strain that can be effectively transferred to the epitaxial MCFO thin films, and thus can result in dramatic changes in the magnetic anisotropy distribution.

The ME effect has been measured for MCFO thin film on $\langle 011\rangle_c$-oriented PMN-29.5PT, where an anisotropic field-induced strain was transferred from substrate to thin film. Remanent magnetization changed in different directions for the two in-plane directions: decreasing along IP$\langle 0-11\rangle_c$ and increasing along IP$\langle 100\rangle_c$ (see Supplemental Material [37]).

Figures 7(a) and 7(b) summarize the field-dependent strains for PMN-PT crystals of different compositions and orientations. The specific electric field on each sample was determined by the threshold E value for polarization rotation/reorientation. A large IP strain of $\varepsilon \approx -0.68\%$ was observed in $\langle 001\rangle_c$-oriented PMN-40PT under $E = 15$ kV/cm. However, this was a one-time effect that could not be reversed by E. On the contrary, a reversible strain of $\varepsilon \approx -0.56\%$ along IP $\langle 100\rangle_c$ was found for $\langle 011\rangle_c$-oriented PMN-29.5PT, which could easily be modulated by E. The reversible IP strain for $\langle 001\rangle_c$-oriented PMN-30PT was very small ($\varepsilon \approx -0.02\%$).

Figure 7(c) summarizes the magnetization squareness modulation results for the heterostructures with different electric-field histories. IP$\langle 100\rangle_c$ is selected here as the direction for comparisons. For MCFO film on $\langle 001\rangle_c$ PMN-30PT, the value of $|\Delta R_M|$ was stable but small ($|\Delta R_M| = 0.01$). During the first measurement cycle of MCFO on $\langle 001\rangle_c$ PMN-40PT and on $\langle 011\rangle_c$ PMN-29.5PT, large-field-induced strains resulted in large changes in the distribution of the magnetic anisotropy: $|\Delta R_M| = 0.128$ and 0.268, respectively. However, during

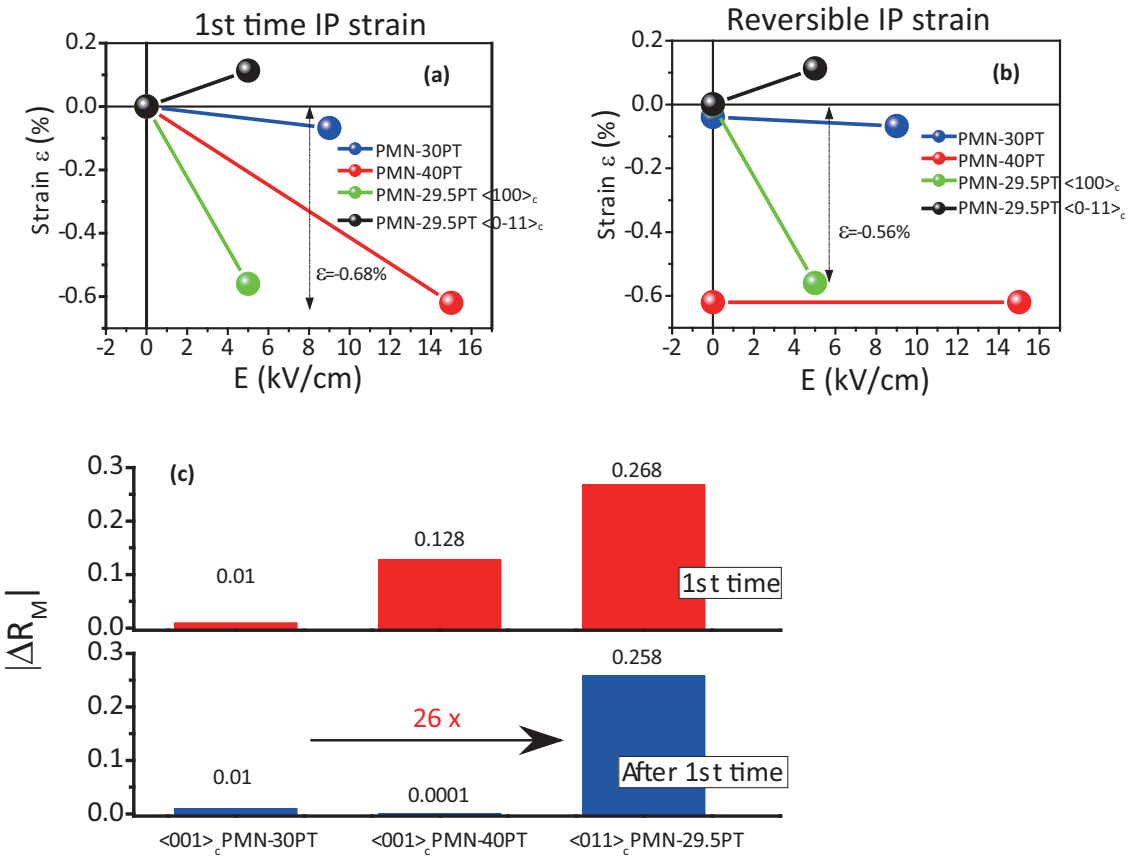

FIG. 7. (Color online) Field-dependent strain amplitudes in PMN-PT single crystals with different composition and characterizing directions at the first time (a) and after the first time (b). (c) Field-dependent magnetization squareness in MCFO films on different PMN-PT single crystals.

the second measurement cycle, the field-induced reversible strain in PMN-40PT was small, and thus $|\Delta R_M| = 0.0001$, as shown in Fig. 7(c). On the contrary, the reversible strain for PMN-29.5PT is high during the second cycle due to the relaxation of the field-induced O phase. Accordingly, the value of $|\Delta R_M| = 0.258$ during the second measurement cycle [Fig. 7(c)] was just as high as that in the first cycle. Furthermore, this value was about 26 times that of MCFO on $\langle 001 \rangle_c$ PMN-30PT. The dramatic difference in the value of $|\Delta R_M|$ shows that changes of $|\Delta R_M|$ are not only related to the strain value along that specific direction, but are also related to the symmetry of the interface strain that has been transferred from the substrate to the epitaxial thin film. The MCFO thin film has a large magnetic shape anisotropy along the in-plane direction, owing to the drastic dimension difference between length and thickness directions, and thus the magnetic moments have been confined in plane even before application of electric field. Therefore the electric-field-induced uniform IP magnetic strain anisotropy in MCFO on $\langle 001 \rangle_c$ PMN-30PT has to compete with magnetic shape anisotropy to induce a change in the magnetization squareness along both IP and OP direction. For MCFO on $\langle 011 \rangle_c$ PMN-29.5PT, the magnetic strain anisotropy decreases along IP$\langle 0{-}11 \rangle$ due to a tensile strain, whereas it increases along IP$\langle 100 \rangle$ due to a compressive strain. No magnetic shape anisotropy difference exists between the two in-plane directions. Therefore, the uniaxial in-plane strain in $\langle 011 \rangle_c$ PMN-29.5PT is much more effective compared with a relatively uniform strain in $\langle 001 \rangle_c$-oriented PMN-PT in the concern of magnetic property modulation.

In summary, we have systematically studied the field-induced strain in epitaxial MCFO films on PMN-PT single crystals with different initial phase stabilities and crystal orientations. MCFO films on $\langle 001 \rangle_c$ PMN-30PT and $\langle 011 \rangle_c$ PMN-29.5PT showed reversible strains due to relaxation of the field-induced phases. The change in magnetization squareness of MCFO on $\langle 011 \rangle_c$ PMN-29.5PT is about 26 times of that on $\langle 001 \rangle_c$ PMN-30PT due to competing magnetic strain and shape anisotropies. It is unambiguous that the uniaxial strain in $\langle 011 \rangle_c$-oriented PMN-29.5PT is much more effective in controlling the direction of related properties, e.g., magnetization reversal, conductivity, electron mobility, etc. The strain in $\langle 001 \rangle_c$ PMN-40PT is a one-time effect. These findings are generally applicable to all epitaxial films on piezoelectric single-crystal substrates, where strain engineering might be used for exploration of new memory and logic devices based on multiferroic heterostructures.

ACKNOWLEDGMENT

This work was supported by the U.S. Department of Energy (Award No. DE-FG02-06ER46290).

[1] A. D. Rata, A. Herklotz, K. Nenkov, L. Schultz, and K. Dörr, Phys. Rev. Lett. **100**, 076401 (2008).

[2] S. A. Harrington, J. Zhai, S. Denev, V. Gopalan, H. Wang, Z. Bi, S. A. T. Redfern, S.-H. Baek, C. W. Bark, C.-B. Eom, Q. Jia, M. E. Vickers, and J. L. MacManus-Driscoll, Nat. Nanotechnol. **6**, 491 (2011).

[3] R. O. Cherifi, V. Ivanovskaya, L. C. Phillips, A. Zobelli, I. C. Infante, E. Jacquet, V. Garcia, S. Fusil, P. R. Briddon, N. Guiblin, A. Mougin, A. A. Uenal, F. Kronast, S. Valencia, B. Dkhil, A. Barthelemy, and M. Bibes, Nat. Mater. **13**, 345 (2014).

[4] J. Li, Z. Shan, and E. Ma, MRS Bull. **39**, 108 (2014).

[5] M. D. Biegalski, K. Dorr, D. H. Kim, and H. M. Christen, Appl. Phys. Lett. **96**, 151905 (2010).

[6] Z. Wang, Y. Wang, W. Ge, J. Li, and D. Viehland, Appl. Phys. Lett. **103**, 132909 (2013).

[7] Z. Wang, Y. Zhang, R. Viswan, Y. Li, H. Luo, J. Li, and D. Viehland, Phys. Rev. B **89**, 035118 (2014).

[8] J. X. Zhang, Q. He, M. Trassin, W. Luo, D. Yi, M. D. Rossell, P. Yu, L. You, C. H. Wang, C. Y. Kuo, J. T. Heron, Z. Hu, R. J. Zeches, H. J. Lin, A. Tanaka, C. T. Chen, L. H. Tjeng, Y. H. Chu, and R. Ramesh, Phys. Rev. Lett. **107**, 147602 (2011).

[9] K. J. Choi, M. Biegalski, Y. L. Li, A. Sharan, J. Schubert, R. Uecker, P. Reiche, Y. B. Chen, X. Q. Pan, V. Gopalan, L. Q. Chen, D. G. Schlom, and C. B. Eom, Science **306**, 1005 (2004).

[10] M. Liu, B. M. Howe, L. Grazulis, K. Mahalingam, T. Nan, N. X. Sun, and G. J. Brown, J. Adv Mater. **25**, 4886 (2013).

[11] T. Wu, A. Bur, K. Wong, J. L. Hockel, C.-J. Hsu, H. K. D. Kim, K. L. Wang, and G. P. Carman, J. Appl. Phys. **109**, 07D732 (2011).

[12] I. Bozovic, G. Logvenov, I. Belca, B. Narimbetov, and I. Sveklo, Phys. Rev. Lett. **89**, 107001 (2002).

[13] J. P. Locquet, J. Perret, J. Fompeyrine, E. Machler, J. W. Seo, and G. Van Tendeloo, Nature **394**, 453 (1998).

[14] Z. Wang, Y. Yang, R. Viswan, J. Li, and D. Viehland, Appl. Phys. Lett. **99**, 043110 (2011).

[15] Z. Wang, R. Viswan, B. Hu, J.-F. Li, V. G. Harris, and D. Viehland, J. Appl. Phys. **111**, 034108 (2012).

[16] C. W. Huang, W. Ren, N. Viet Cuong, Z. Chen, J. Wang, T. Sritharan, and L. Chen, Adv. Mater. **24**, 4170 (2012).

[17] L. Yan, Y. Yang, Z. Wang, Z. Xing, J. Li, and D. Viehland, J. Mater. Sci. **44**, 5080 (2009).

[18] Z. Wang, Y. Li, R. Viswan, B. Hu, V. G. Harris, J. Li, and D. Viehland, ACS Nano **7**, 3447 (2013).

[19] L. Yan, Z. Xing, Z. Wang, T. Wang, G. Lei, J. Li, and D. Viehland, Appl. Phys. Lett. **94**, 192902 (2009).

[20] Z. Wang, L. Yan, Y. Yang, J.-F. Li, J. Das, A. L. Geiler, A. Yang, Y. Chen, V. G. Harris, and D. Viehland, J. Appl. Phys. **109**, 034102 (2011).

[21] L. Yan, Z. Wang, Z. Xing, J. Li, and D. Viehland, J. Appl. Phys. **107**, 064106 (2010).

[22] Z. Wang, R. Viswan, B. Hu, V. G. Harris, J.-F. Li, and D. Viehland, Phys. Status Solidi RRL **6**, 92 (2012).

[23] M. Li, Z. Wang, Y. Wang, J. Li, and D. Viehland, Appl. Phys. Lett. **102**, 082404 (2013).

[24] B. Noheda, D. E. Cox, G. Shirane, J. Gao, and Z. G. Ye, Phys. Rev. B **66**, 054104 (2002).

[25] H. Cao, F. Bai, N. Wang, J. Li, D. Viehland, G. Xu, and G. Shirane, Phys. Rev. B **72**, 064104 (2005).

[26] S. E. Park and T. R. Shrout, J. Appl. Phys. **82**, 1804 (1997).

[27] W. Eerenstein, M. Wiora, J. L. Prieto, J. F. Scott, and N. D. Mathur, Nat. Mater. **6**, 348 (2007).

[28] H. X. Fu and R. E. Cohen, Nature **403**, 281 (2000).

[29] F. M. Bai, J. F. Li, and D. Viehland, J. Appl. Phys. **97**, 054103 (2005).

[30] See Supplemental Material at http://link.aps.org/supplemental/10.1103/PhysRevB.90.134103 for the M-H loops of MCFO on $\langle 001\rangle_c$ PMN-30PT.

[31] See Supplemental Material at http://link.aps.org/supplemental/10.1103/PhysRevB.90.134103 for the M-H loops of MCFO on $\langle 001\rangle_c$ PMN-40PT.

[32] Y. Lu, D. Y. Jeong, Z. Y. Cheng, Q. M. Zhang, H. S. Luo, Z. W. Yin, and D. Viehland, Appl. Phys. Lett. **78**, 3109 (2001).

[33] M. Shanthi, S. M. Chia, and L. C. Lim, Appl. Phys. Lett. **87**, 202902 (2005).

[34] A. E. Renault, H. Dammak, G. Calvarin, P. Gaucher, and M. P. Thi, J. Appl. Phys. **97**, 044105 (2005).

[35] Y. P. Guo, H. S. Luo, T. H. He, H. Q. Xu, and Z. W. Yin, Jpn. J. Appl. Phys. **41**, 1451 (2002).

[36] Z. Wang, Y. Zhang, Y. Wang, Y. Li, H. Luo, J. Li, and D. Viehland, ACS Nano **8**, 7793 (2014).

[37] See Supplemental Material at http://link.aps.org/supplemental/10.1103/PhysRevB.90.134103 for the M-H loops of MCFO on $\langle 011\rangle_c$ PMN-29.5PT.